HHS Public Access

Author manuscript

Bone. Author manuscript; available in PMC 2016 October 01.

Published in final edited form as:

Bone. 2015 October ; 79: 8–14. doi:10.1016/j.bone.2015.05.020.

Fatigue-Induced Microdamage in Cancellous Bone Occurs Distant from Resorption Cavities and Trabecular Surfaces

M.G. Goff[1,2], **F.M. Lambers**[2], **T.M. Nguyen**[2], **J. Sung**[3], **C.M. Rimnac**[4], and **C.J. Hernandez**[1,2,5]

[1]Department of Biomedical Engineering, Cornell University, Ithaca, NY, USA

[2]Sibley School of Mechanical and Aerospace Engineering, Cornell University, Ithaca, NY, USA

[3]College of Veterinary Medicine, Cornell University, Ithaca, NY, USA

[4]Departments of Mechanical and Aerospace Engineering and Orthopaedics, Case Western Reserve University, Cleveland, OH, USA

[5]Hospital for Special Surgery, New York City, NY, USA

Abstract

Impaired bone toughness is increasingly recognized as a contributor to fragility fractures. At the tissue level, toughness is related to the ability of bone tissue to resist the development of microscopic cracks or other tissue damage. While most of our understanding of microdamage is derived from studies of cortical bone, the majority of fragility fractures occur in regions of the skeleton dominated by cancellous bone. The development of tissue microdamage in cancellous bone may differ from that in cortical bone due to differences in microstructure and tissue ultrastructure. To gain insight into how microdamage accumulates in cancellous bone we determined the changes in number, size and location of microdamage sites following different amounts of cyclic compressive loading. Human vertebral cancellous bone specimens (n=32, 10 male donors, 6 female donors, age 76 ± 8.8, mean ± SD) were subjected to sub-failure cyclic compressive loading and microdamage was evaluated in three-dimensions. Only a few large microdamage sites (the largest 10%) accounted for 70% of all microdamage caused by cyclic loading. The number of large microdamage sites was a better predictor of reductions in Young's modulus caused by cyclic loading than overall damage volume fraction (DV/BV). The majority of microdamage volume (69.12 ± 7.04%) was located more than 30 μm (the average erosion depth) from trabecular surfaces, suggesting that microdamage occurs primarily within interstitial regions of cancellous bone. Additionally, microdamage was less likely to be near resorption cavities than other bone surfaces ($p<0.05$), challenging the idea that stress risers caused by resorption cavities influence fatigue failure of cancellous bone. Together, these findings suggest that reductions in apparent level mechanical performance during fatigue loading are the result of only a few large

Corresponding Address: Christopher J. Hernandez, Ph.D., 219 Upson Hall, Cornell University, Ithaca, NY 14853, Phone: (607) 255-5129, Fax: (607) 255-1222, cjh275@cornell.edu.

Authors' roles: Conceived and designed the experiments: MGG, FML, CMR, CJH. Analyzed data: MGG, TMN, JJ, FML. Wrote the paper: MGG, CJH. Critical revision and final approval of the manuscript: MGG, FML, TMN, JJ, CMR, CJH.

microdamage sites and that microdamage accumulation in fatigue is likely dominated by heterogeneity in tissue material properties rather than stress concentrations caused by micro-scale geometry.

Keywords

Microdamage; Bone Mechanics; Cancellous Bone; Biomechanics; Bone Quality

1.0 INTRODUCTION

Impaired material toughness and resistance to crack growth in bone has been implicated as a cause of fragility fractures in patients with diabetes and patients submitted to long-term bisphosphonate treatment [1, 2]. Examination of microdamage is the primary means of assessing tissue material toughness and resistance to crack growth [3-5]. Most of our understanding of microdamage is derived from studies of cortical bone. However, fragility fractures typically occur in regions of the skeleton dominated by cancellous bone [6, 7].

Cancellous bone microarchitecture and ultrastructure differs from that in cortical bone in ways that may influence the development of microdamage. In cortical bone, microdamage forms primarily in interstitial tissue and microdamage morphology may be influenced by structures such as the cement lines that surround osteons [4, 5, 8]. In cancellous bone, interstitial tissue is present in the central regions of trabeculae, distant from the trabecular surfaces [9], yet trabecular surfaces are expected to show the greatest tissue stresses due to bending and torsion of individual trabeculae during loading. Additionally, the orientation of cement lines in cancellous bone differs from that in cortical bone since cancellous bone does not have osteons per se (instead it has “hemi-osteons”) [10]. Furthermore, remodeling in cancellous bone causes the generation of resorption cavities, which are believed to act as stress risers and encourage the initiation and propagation of microdamage [11, 12].

Characterization of the development of microdamage in cancellous bone requires measurement of the number and size of individual microdamage sites. While there have been many studies of microdamage in cancellous bone [13-18] most studies have evaluated microdamage using two dimensional methods that cannot accurately measure the number or size of microdamage sites or provide information about the location of microdamage sites relative to the rest of the trabecular microstructure due to the lack of out-of-plane information [19]. We and others have used three-dimensional imaging methods to examine the overall amounts of microdamage generated in cancellous bone following loading [20-22], but the number, size and location of microdamage sites relative to the bone surface or resorption cavities has not been reported. Hence, it is unclear how the number and size of microdamage sites is related to the amount of applied loading.

The long-term goal of the current work is to understand how microdamage in cancellous bone contributes to cancellous bone failure and clinical fracture. Specifically, in the current study we determine: 1) the relationship between the number and size of microdamage sites, and reductions in biomechanical performance (Young’s modulus) following different

amounts of fatigue loading; and 2) the location of microdamage relative to bone surfaces and resorption cavities.

2.0 METHODS

We performed an extended analysis of specimens described in a previous study [20]. In section 2.1 we briefly review the experimental methods of the prior study and in sections 2.2-2.5 we describe the methods novel to the current study.

2.1 Study design

Specimens were collected from the L3 vertebral bodies of 16 donors (10 male, 6 female, 62-92 years of age, tissue from NDRI, Philadelphia, PA). The donors had no history of metabolic bone disease and displayed no obvious vertebral deformities. Cylinders of cancellous bone, 8 mm in diameter and nominally 25-30 mm height oriented in the cranial-caudal direction, were collected (2 specimens per donor, n=32 specimens total). Specimens were stored at −20 °C and hydration was maintained throughout the experiments. Specimens were press fit into brass endcaps with cyanoacrylate glue (as previously described [23]) and submitted to cyclic loading at 4 Hz between 0N and a normalized stress value (σ/E_0) of 0.0035 (where E_0 is the initial apparent Young's modulus and σ is the load divided by the cross sectional area in load control). Cyclic loading was stopped at a predetermined reduction in the apparent Young's modulus (Figure 1). The reductions in apparent Young's modulus were selected to observe microdamage in the secondary and tertiary phases of the fatigue life [20]. One group of specimens (n=5) was placed in the loading fixture but no load was applied. Following loading, the specimens were stained with lead uranyl acetate to identify microdamage [21]. Three-dimensional images of each cylinder of cancellous bone were acquired through micro-computed tomography to characterize trabecular microarchitecture and stained microdamage. A region of interest (the central 8 mm diameter, 10.2 mm height) was scanned using a micro-computed tomography device (Versa XRM-520, Xradia, Pleasanton, CA) in air at an energy of 100 kVp, a current of 90 μA and an isotropic voxel size of 10 μm. A Gaussian filter (sigma = 1.2, support = 1) was applied to the images and bone was segmented using a global threshold determined with the Otsu method. To segment microdamage from bone, manual thresholds were chosen by an observer blinded to the amount of loading the specimen received. Stained objects smaller than 10,000 μm^3 (approximately the volume of 20 osteocyte lacunae) were considered noise and removed from the images. The volume of stained microdamage in the entire specimen was characterized as the damaged bone volume fraction (DV/BV).

2.2 Number, Size and Location of Microdamage

In cortical bone, the growth of individual microdamage sites (cracks) is observed by introducing notches into specimens and tracking the growth of individual cracks while cyclic loading is applied [24]. In cancellous bone, the trabecular microstructure prevents direct observation of microdamage during mechanical testing. The accumulation of microdamage, however, occurs through a combination of the creation of new microdamage sites and/or the increase in the size of microdamage sites. The relative contribution of new microdamage sites and increases in size of microdamage sites can be inferred by examining

changes in the distribution of microdamage site sites (as illustrated in a histogram, Figure 2). The creation of new microdamage sites is expected to increase the height of the histogram, while an increase in the size of existing microdamage sites is expected to increase the right hand side of the histogram.

In cancellous bone, interstitial tissue is present in the central cores of trabeculae [9]. To determine if microdamage occurs preferentially within the interstitial regions of cancellous bone, the proportion of microdamage located more than 30 μm from the bone surface was examined (the average maximum resorption cavity depth in human vertebral trabecular bone is 30 μm [10]). Additionally, to determine if microdamage was more concentrated in the interstitial tissue, the damage volume fraction of tissue near the surface (DV_{near}/BV_{near}) and the damage volume fraction of tissue distant from the surface ($DV_{distant}/BV_{distant}$) were determined.

2.3 Spatial correlation of microdamage and resorption cavities

Resorption cavities on the trabecular surfaces have been implicated as stress risers that might promote microdamage formation [11, 25, 26]. To determine the effects of resorption cavities on the location of microdamage, a subset of the specimens (n=9) were submitted to higher resolution imaging (Figure 1). A second micro-computed tomography image was collected of the central region (3 mm diameter, 3 mm height) of each of these nine specimens using the two stage magnification capability of a micro-computed tomography device (Versa XRM-520, Xradia, Pleasanton, CA) to achieve an isotropic voxel size of 1.5 μm, a resolution sufficient to detect individual resorption cavities based on bone surface texture [27]. Images were collected in air at an energy of 80 kVp, and a current of 7 A. Global thresholds for bone and microdamage were calculated using the two material Otsu method [28]. As above, stained microdamage sites smaller than 10,000 μm^3 were removed from the images as noise. Additionally, to eliminate non-specific surface staining (thin layers of stain that occur on bone surfaces without microdamage), lead uranyl acetate staining within 5 μm of the surface of the trabeculae was disregarded as noise. Resorption cavities were identified based on bone surface texture (the “scalloped surface”) and traced in three-dimensions by observers blinded to the presence of microdamage ([10], Figure 3). Image processing and analysis were performed using custom software written for use with Matlab (version 7.11.0, Mathworks, Natick, MA, USA) and image visualization and tracing was performed using Amira (version 5.3, Visage Imaging, San Diego, CA, USA).

The spatial correlation between microdamage and resorption cavities was determined using two different methodologies: 1) a volume based method; and 2) an object based method [29]. The volume based method determined the degree to which microdamage volume was more likely to be near eroded surfaces than other bone surfaces. The volume based spatial correlation was expressed as the ratio of the amount of damage volume near eroded surfaces to that of an equal amount of bone volume (selected at random) near eroded surfaces. A ratio of 1.0 indicated no spatial correlation, a ratio greater than 1.0 indicated a positive spatial correlation (eroded surfaces were more likely to be near damage volume than other bone volume) and a value less than 1.0 indicated negative spatial correlation (eroded surfaces were less likely to be near damage volume than other bone volume). The volume based

spatial correlation was then repeated to ask the converse question: if eroded surface was more likely to be near microdamage than other bone volume. The object based spatial correlation was expressed as the percentage of microdamage sites near eroded surfaces and as the percentage of resorption cavities with microdamage nearby. For both spatial correlation methods, proximity was determined at distances ranging from 8 μm to 133 μm (the average trabecular thickness).

2.4 Statistical analyses

Regression analysis was used to determine the relationship between the number and size of microdamage sites and reductions in Young's modulus associated with fatigue loading. Donor was included as a random effect to take into account the use of multiple specimens from each donor. Differences in the damage volume fraction near and away from the bone surface were determined using a paired t-test. The spatial correlations determined using the volume based method were tested for a difference from 1.0 using a paired t-test, (a value of 1.0 indicated no spatial correlation). Statistical tests were conducted using JMP (v.20 9, SAS Institute Inc., Cary, NC, USA).

3.0 RESULTS

Specimens experiencing greater reductions in biomechanical performance showed increased amounts of microdamage (Figure 4) but no significant increases in the number of microdamage sites or median microdamage site size. However, histograms of microdamage site size showed a shift to the right hand side in specimens submitted to greater amounts of fatigue loading, indicating an increased number of large microdamage sites (Figure 5). For the purposes of this analysis, a microdamage site was characterized as "large" if it was more than 10^6 μm^3 in volume (the 90^{th} percentile of microdamage site volume observed in unloaded specimens). While only a small percentage of the microdamage sites were large by this criterion (9.9% ± 4.9%, mean ± SD), large microdamage sites accounted for the majority of the microdamage volume (69% ± 14%) and the number of large microdamage sites was strongly correlated with the overall damage volume fraction (R^2_{adj}=0.95, $p<0.001$, Figure 4C). Additionally, variance in the reduction in Young's modulus was better explained by the number of large microdamage sites (R^2_{adj}=0.39, $p<0.001$, Figure 4B) than by the total amount of microdamage (R^2_{adj}=0.20, $p<0.01$, Figure 4A). Reductions in Young's modulus during cyclic loading were not correlated with the number of microdamage sites ($p=0.16$, Figure 4D) or the median size of microdamage sites ($p=0.95$). Donor age was not correlated with the number or size of microdamage sites nor was donor age a covariate when comparing microdamage site number and size to reductions in Young's modulus.

Volume based spatial correlations indicated that microdamage was less likely to be near eroded bone surfaces than bone surfaces selected at random ($p<0.05$, Figure 6A). Eroded surfaces were not more or less likely to have microdamage nearby (Figure 6B). The object-based spatial correlation indicated that most resorption cavities had microdamage nearby (Figure 7A), but few microdamage sites had resorption cavities nearby (Figure 7B). The majority (69.12 ± 7.04%) of the microdamage generated by fatigue loading was distant from

the bone surface ($DV_{distant}/DV$). Microdamage was more concentrated distant from the bone surface ($DV_{distant}/BV_{distant}$ = 2.23 ± 1.87%) than near the trabecular surface (DV_{near}/BV_{near} = 0.96 ± 0.92%, $p<0.001$).

4.0 DISCUSSION

Our finding that fatigue loading of cancellous bone leads to the creation of many small microdamage sites but most of the microdamage volume occurs in just a few large microdamage sites is consistent with the idea that bone tissue limits the growth of microdamage sites. Large microdamage sites were also more highly correlated with reductions in Young's modulus, suggesting that mechanical failure at only a few locations within the cancellous bone structure can greatly impair apparent level mechanical performance.

An increase in the number of microdamage sites following greater amounts of fatigue loading suggests initiation of new microdamage sites, while the increase in size of microdamage sites suggests the propagation or coalescence of microdamage sites later in the fatigue life. Direct observation of microdamage extension within cancellous bone or other cellular solids has not yet been reported and would be required to assess the initiation and propagation of microdamage. The current study did not examine microdamage morphology (crack-like v. diffuse). While some have used the ratio of the damage surface area to the damage volume (DS/DV) [32] to identify more crack-like and more diffuse like microdamage sites, because the measurement is not dimensionless (units 1/mm), DS/DV is also influenced by microdamage site size. Given the large distribution of microdamage site size in the current study, DS/DV could not reliably differentiate among microdamage morphologies. Additional analysis of microdamage morphology would be required to separate microcracks from diffuse damage.

Both the creation of new microdamage sites and the increase in size of existing microdamage sites are a result of both local tissue stresses/strains and local tissue material properties [31]. The current study examined two microstructural traits associated with increased local tissue stress/strain: resorption cavities and trabecular surfaces. Resorption cavities have received considerable attention as stress risers within cancellous bone and finite element models suggest that resorption cavities can reduce cancellous bone stiffness and strength more than would be expected from changes in bone volume fraction [11, 12, 33]. Interpretation of the spatial correlation between resorption cavities and microdamage, however, was not straightforward. In particular, our observations that microdamage volume was preferentially distant from eroded surfaces (Figure 6A), yet most resorption cavities had a microdamage site nearby (Figure 7A) at first appears contradictory. Our examination of the microdamage site size distribution (Figure 5), however, suggests that there were many small specks of stained microdamage in each specimen (some potentially image noise or non-specific staining), but that the large and most mechanically relevant microdamage sites were preferentially distant from resorption cavities.

The negative spatial correlation between microdamage and resorption cavities was unexpected because resorption cavities have been shown to cause local stress concentrations

[11, 12]. One possible explanation is that resorption cavities in our study occurred preferentially in regions of the structure experiencing low nominal stresses such that even with the stress concentrations from resorption cavities, local stresses were not sufficient to promote microdamage. It is possible that the presence of cavities on trabeculae may alter the load distribution within cancellous bone resulting in reduced stresses at resorption cavities. Another possible explanation is that local tissue material properties near resorption cavities influence microdamage generation. Since individual trabeculae undergo bending and torsion during apparent compression, we would expect local tissue stresses to be greater near the bone surface and therefore microdamage to be closer to the surface [35], but our analysis demonstrated just the opposite, that microdamage occurs preferentially distant from the bone surface. We suggest that the location and size of microdamage may be more influenced by tissue material properties than stress concentrations caused by micro-scale geometry.

Cancellous bone tissue displays considerable heterogeneity in tissue age and material properties. Since bone remodeling in cancellous bone occurs at trabecular surfaces, relatively younger tissue is located near the surface of trabeculae and older interstitial regions are found at the center of trabeculae [36]. We found microdamage in cancellous bone primarily distant from the bone surface, regions that we expect to contain older tissue. Our findings are consistent with previous studies that have shown that microdamage forms near the center of trabeculae [14], and are also consistent with observations in cortical bone that microdamage forms primarily in interstitial regions [4, 5, 8]. Interstitial bone tissue has been shown to have greater tissue age, reduced toughness [37], and is both stiffer and harder than the bone tissue near the surface of trabeculae [38, 39]. Therefore, the negative spatial correlation between resorption cavities and microdamage in the current study may be a result of more ductile tissue near trabecular surfaces (due to younger local tissue age). However, increased non-enzymatic glycation (a trait associated with increased tissue brittleness [32]) has been shown to impair osteoclastic bone resorption in vitro [40] and is negatively correlated with resorption cavities in cortical bone [41]. If such a negative correlation also exists in cancellous bone it could also explain the negative correlation between microdamage and resorption cavities we observed. The possibility of a link between local tissue material properties and localization of bone resorption is intriguing and requires further study.

A strength of the study was that both microdamage sites and resorption cavities were characterized in three dimensions. Three dimensional analysis of both microdamage and resorption cavities enables characterization of the number and size of microdamage sites and reduces the variability in the measures by using the entire specimen [42]. There were also some limitations that must be considered when interpreting our findings. First, microdamage was observed using lead uranyl acetate staining. While lead uranyl acetate stains bone tissue damage, some have proposed that lead uranyl acetate stain may have limited penetration into bone surfaces [43]. However, since the majority of the microdamage we observed was distant from the bone surface, it is unlikely that limited diffusion of lead uranyl acetate influenced our conclusions. Second, as mentioned above the observed changes in microdamage site number and size suggest changes in microdamage initiation and propagation during fatigue loading, but the current study does not directly measure propagation of individual microdamage sites. The difference between our approach and

direct observation of microdamage propagation was analogous to the differences between a cross-sectional clinical study (current study) and a longitudinal clinical study (where extension of individual microdamage sites is observed directly). Methods of observing the propagation of individual microdamage sites in cancellous bone during mechanical loading are not currently available, but would be useful for understanding tissue brittleness in cancellous bone.

In conclusion, we have demonstrated that degradation in biomechanical performance of trabecular bone during fatigue loading can be attributed to a few, large microdamage sites. Microdamage appears primarily distant from resorption cavities and the trabecular surface and is consistent with the idea that the locations of microdamage initiation and propagation under fatigue loading is determined more by tissue material properties/tissue heterogeneity than stress concentrations associated with microscale geometry. Our results therefore highlight the importance of tissue material properties in failure processes in cancellous bone.

ACKNOWLEDGEMENTS

Research reported in this publication was supported by the National Institute of Arthritis and Musculoskeletal and Skin Diseases of the National Institutes of Health (U.S) under Award Number AR057362 (PI CJH). The content is solely the responsibility of the authors and does not necessarily represent the official views of the National Institutes of Health. We acknowledge use of human vertebral bodies provided by the National Disease Research Interchange (NDRI), with support from NIH grant 8U42OD011158-22. For technical support, we thank Garry Brock, Kathy Ehlert, Daniel Brooks and Christopher Chapa for technical assistance and Mark Riccio and Fred von Stein for imaging assistance.

REFERENCES

[1]. Shane E, Burr D, Abrahamsen B, Adler RA, Brown TD, Cheung AM, Cosman F, Curtis JR, Dell R, Dempster DW, Ebeling PR, Einhorn TA, Genant HK, Geusens P, Klaushofer K, Lane JM, McKiernan F, McKinney R, Ng A, Nieves J, O'Keefe R, Papapoulos S, Howe TS, van der Meulen MC, Weinstein RS, Whyte MP. Atypical subtrochanteric and diaphyseal femoral fractures: second report of a task force of the American Society for Bone and Mineral Research. J Bone Miner Res. 2014; 29:1–23. [PubMed: 23712442]

[2]. de Waard EA, van Geel TA, Savelberg HH, Koster A, Geusens PP, van den Bergh JP. Increased fracture risk in patients with type 2 diabetes mellitus: An overview of the underlying mechanisms and the usefulness of imaging modalities and fracture risk assessment tools. Maturitas. 2014

[3]. Vashishth D, Behiri JC, Bonfield W. Crack growth resistance in cortical bone: concept of microcrack toughening. J Biomech. 1997; 30:763–9. [PubMed: 9239560]

[4]. Carter DR, Hayes WC. Compact bone fatigue damage: a microscopic examination. Clin Orthop Relat Res. 1977:265–74. [PubMed: 912990]

[5]. Saha S. Longitudinal Shear Properties of Human Compact Bone and Its Constituents, and Associated Failure Mechanisms. J Mater Sci. 1977; 12:1798–1806.

[6]. Link TM. Osteoporosis imaging: state of the art and advanced imaging. Radiology. 2012; 263:3–17. [PubMed: 22438439]

[7]. Griffith JF, Genant HK. New advances in imaging osteoporosis and its complications. Endocrine. 2012; 42:39–51. [PubMed: 22618377]

[8]. O'Brien FJ, Taylor D, Clive Lee T. The effect of bone microstructure on the initiation and growth of microcracks. J Orthop Res. 2005; 23:475–80. [PubMed: 15734265]

[9]. Birkenhager-Frenkel DH, Nigg AL, Hens CJ, Birkenhager JC. Changes of interstitial bone thickness with age in men and women. Bone. 1993; 14:211–6. [PubMed: 8363859]

[10]. Goff MG, Slyfield CR, Kummari SR, Tkachenko EV, Fischer SE, Yi YH, Jekir MG, Keaveny TM, Hernandez CJ. Three-dimensional characterization of resorption cavity size and location in human vertebral trabecular bone. Bone. 2012; 51:28–37. [PubMed: 22507299]

[11]. Hernandez CJ. How can bone turnover modify bone strength independent of bone mass? Bone. 2008; 42:1014–20. [PubMed: 18373970]

[12]. McNamara LM, Van der Linden JC, Weinans H, Prendergast PJ. Stress-concentrating effect of resorption lacunae in trabecular bone. J Biomech. 2006; 39:734–41. [PubMed: 16439243]

[13]. Arthur Moore TL, Gibson LJ. Microdamage accumulation in bovine trabecular bone in uniaxial compression. J Biomech Eng. 2002; 124:63–71. [PubMed: 11873773]

[14]. Fyhrie DP, Schaffler MB. Failure mechanisms in human vertebral cancellous bone. Bone. 1994; 15:105–9. [PubMed: 8024844]

[15]. Nagaraja S, Skrinjar O, Guldberg RE. Spatial correlations of trabecular bone microdamage with local stresses and strains using rigid image registration. J Biomech Eng. 2011; 133:064502. [PubMed: 21744931]

[16]. Moore TL, Gibson LJ. Fatigue microdamage in bovine trabecular bone. J Biomech Eng. 2003; 125:769–76. [PubMed: 14986400]

[17]. Green JO, Wang J, Diab T, Vidakovic B, Guldberg RE. Age-related differences in the morphology of microdamage propagation in trabecular bone. J Biomech. 2011; 44:2659–66. [PubMed: 21880317]

[18]. Lee TC, Arthur TL, Gibson LJ, Hayes WC. Sequential labelling of microdamage in bone using chelating agents. J Orthop Res. 2000; 18:322–5. [PubMed: 10815835]

[19]. Mouton, PR. Unbiased Stereology: A Concise Guide. Johns Hopkins University Press; 2013.

[20]. Lambers FM, Bouman AR, Rimnac CM, Hernandez CJ. Microdamage caused by fatigue loading in human cancellous bone: relationship to reductions in bone biomechanical performance. PLoS One. 2013; 8:e83662. [PubMed: 24386247]

[21]. Tang SY, Vashishth D. A non-invasive in vitro technique for the three-dimensional quantification of microdamage in trabecular bone. Bone. 2007; 40:1259–64. [PubMed: 17329178]

[22]. Karim L, Vashishth D. Role of trabecular microarchitecture in the formation, accumulation, and morphology of microdamage in human cancellous bone. J Orthop Res. 2011; 29:1739–44. [PubMed: 21538510]

[23]. Keaveny TM, Pinilla TP, Crawford RP, Kopperdahl DL, Lou A. Systematic and random errors in compression testing of trabecular bone. J Orthop Res. 1997; 15:101–10. [PubMed: 9066533]

[24]. Bonfield W. Advances in the fracture mechanics of cortical bone. J Biomech. 1987; 20:1071–81. [PubMed: 3323199]

[25]. Hernandez CJ, Gupta A, Keaveny TM. A biomechanical analysis of the effects of resorption cavities on cancellous bone strength. J Bone Miner Res. 2006; 21:1248–55. [PubMed: 16869723]

[26]. Lambers FM, Bouman AR, Tkachenko EV, Keaveny TM, Hernandez CJ. The effects of tensile-compressive loading mode and microarchitecture on microdamage in human vertebral cancellous bone. J Biomech. 2014; 47:3605–3612. [PubMed: 25458150]

[27]. Tkachenko EV, Slyfield CR, Tomlinson RE, Daggett JR, Wilson DL, Hernandez CJ. Voxel size and measures of individual resorption cavities in three-dimensional images of cancellous bone. Bone. 2009; 45:487–92. [PubMed: 19482097]

[28]. Otsu N. Threshold Selection Method from Gray-Level Histograms. Ieee T Syst Man Cyb. 1979; 9:62–66.

[29]. Goff MG, Chang KL, Litts EN, Hernandez CJ. The effects of misalignment during in vivo loading of bone: Techniques to detect the proximity of objects in three-dimensional models. J Biomech. 2014

[30]. Zioupos P, Currey JD. The extent of microcracking and the morphology of microcracks in damaged bone. J Mater Sci. 1994; 29:978–986.

[31]. Launey ME, Buehler MJ, Ritchie RO. On the Mechanistic Origins of Toughness in Bone. Ann Rev of Mat Res. 2010; 40:25–53.

[32]. Tang SY, Vashishth D. Non-enzymatic glycation alters microdamage formation in human cancellous bone. Bone. 2010; 46:148–54. [PubMed: 19747573]

[33]. van Oers RF, van Rietbergen B, Ito K, Huiskes R, Hilbers PA. Simulations of trabecular remodeling and fatigue: is remodeling helpful or harmful? Bone. 2011; 48:1210–5. [PubMed: 21256994]

[34]. Ruff C, Holt B, Trinkaus E. Who's afraid of the big bad Wolff?: "Wolff's law" and bone functional adaptation. Am J Phys Anthropol. 2006; 129:484–98. [PubMed: 16425178]

[35]. Mulder L, van Ruijven LJ, Koolstra JH, van Eijden TM. The influence of mineralization on intratrabecular stress and strain distribution in developing trabecular bone. Ann Biomed Eng. 2007; 35:1668–77. [PubMed: 17605109]

[36]. Qiu S, Rao DS, Palnitkar S, Parfitt AM. Age and distance from the surface but not menopause reduce osteocyte density in human cancellous bone. Bone. 2002; 31:313–8. [PubMed: 12151084]

[37]. Nalla RK, Kruzic JJ, Kinney JH, Ritchie RO. Effect of aging on the toughness of human cortical bone: evaluation by R-curves. Bone. 2004; 35:1240–6. [PubMed: 15589205]

[38]. Burket JC, Brooks DJ, MacLeay JM, Baker SP, Boskey AL, van der Meulen MC. Variations in nanomechanical properties and tissue composition within trabeculae from an ovine model of osteoporosis and treatment. Bone. 2013; 52:326–36. [PubMed: 23092698]

[39]. Mulder L, Koolstra JH, den Toonder JM, van Eijden TM. Intratrabecular distribution of tissue stiffness and mineralization in developing trabecular bone. Bone. 2007; 41:256–65. [PubMed: 17567548]

[40]. Valcourt U, Merle B, Gineyts E, Viguet-Carrin S, Delmas PD, Garnero P. Non-enzymatic glycation of bone collagen modifies osteoclastic activity and differentiation. J Biol Chem. 2007; 282:5691–703. [PubMed: 17142454]

[41]. Ural A, Janeiro C, Karim L, Diab T, Vashishth D. Association between non-enzymatic glycation, resorption, and microdamage in human tibial cortices. Osteoporos Int. 2014

[42]. Ehlert, K.; O'Brien, R.; Hernandez, C. Statistical power in measures of microscopic tissue damage in cancellous bone; Annual Meeting of the American Society for Bone and Mineral Research; 2011; p. M0052

[43]. Brock GR, Kim G, Ingraffea AR, Andrews JC, Pianetta P, van der Meulen MC. Nanoscale examination of microdamage in sheep cortical bone using synchrotron radiation transmission x-ray microscopy. PLoS One. 2013; 8:e57942. [PubMed: 23472121]

Highlights

- Microdamage generated by fatigue loading was examined in three dimensions in human cancellous bone.
- Increases in microdamage volume during fatigue loading were associated with increased size of just a few large microdamage sites.
- The number of large microdamage sites was more strongly related to reductions in stiffness than the overall micro damage volume.
- Microdamage occurred preferentially distant from resorption cavities and near the center of trabecular.
- Our results show that local tissue material properties have a greater influence on micro damage generation than micro-scale stress concentrations.

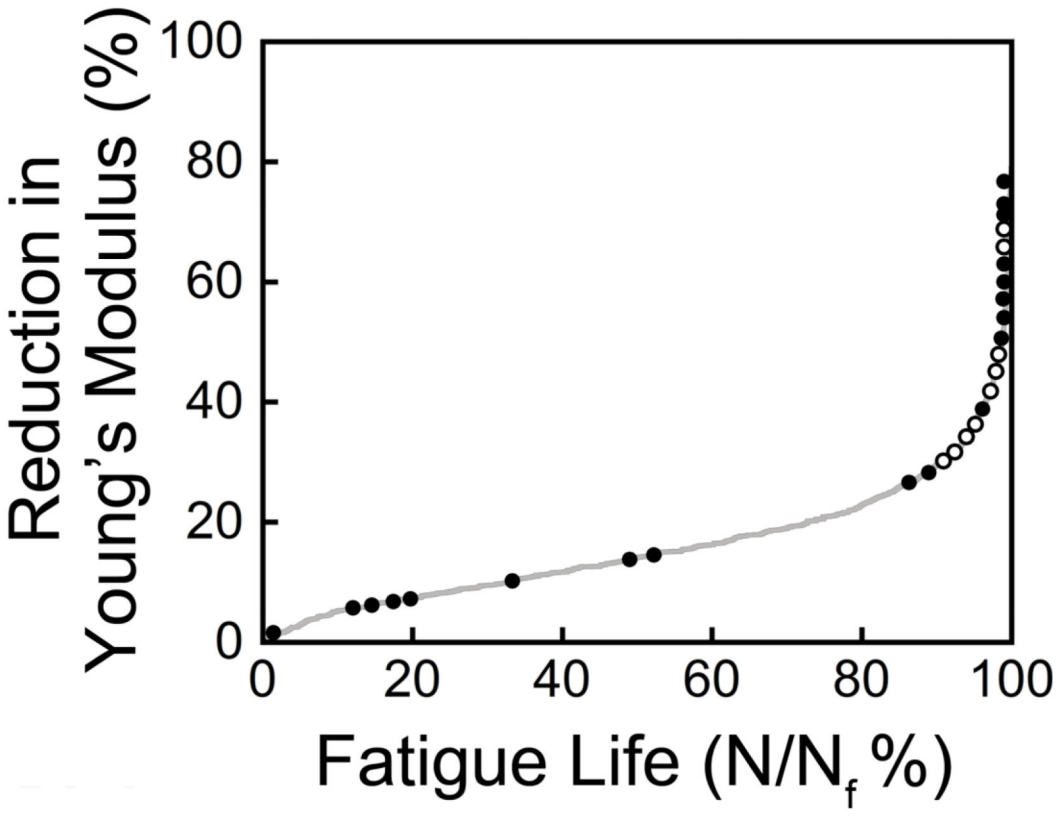

Figure 1.

Cyclic loading was stopped after different amounts of fatigue loading. Each circle, open and closed, represents one specimen (n = 32, 5 specimen were not loaded). The relationship between microdamage sites and resorption cavities was examined in a subset of specimens loaded to the tertiary phase (open circles only, n=9).

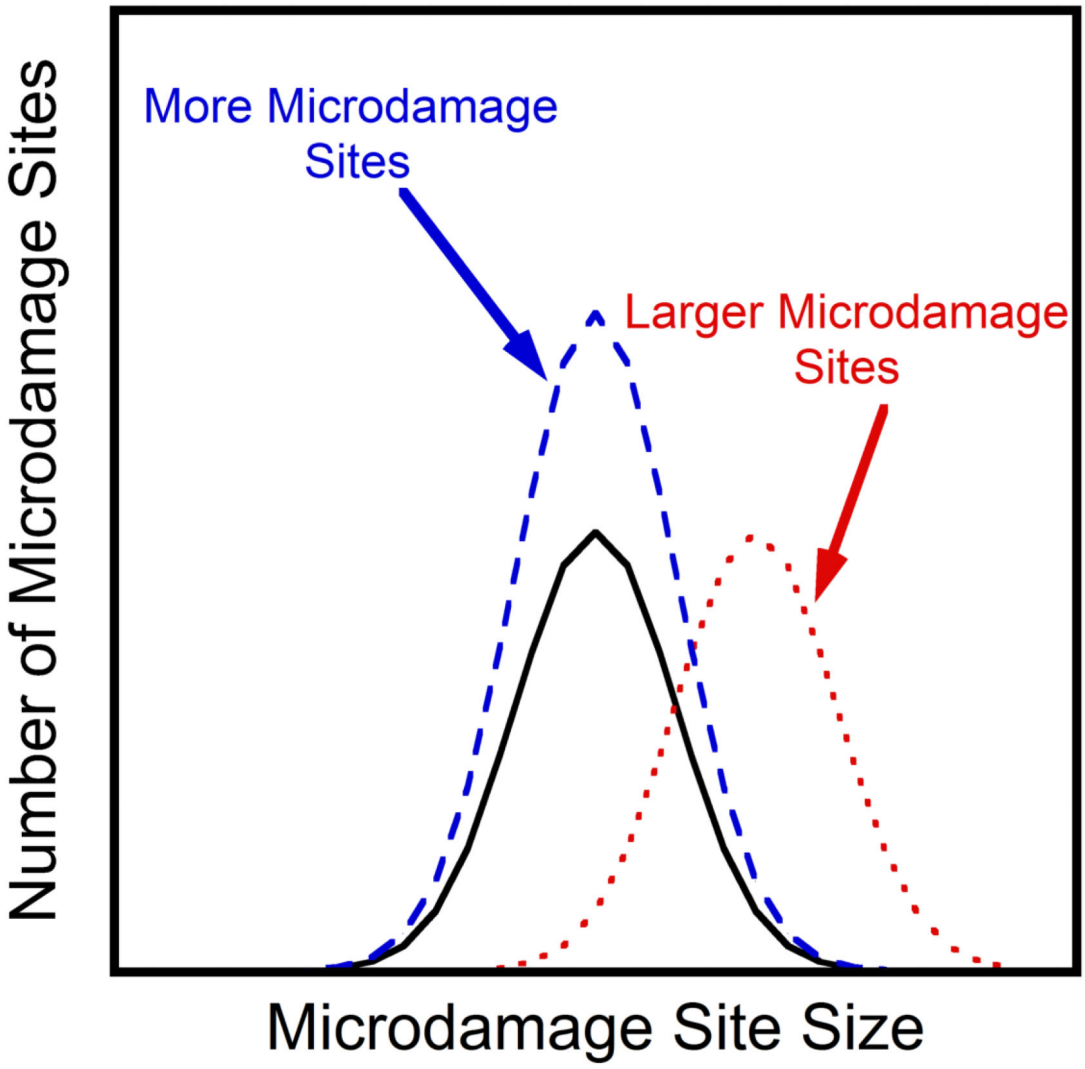

Figure 2.
Hypothetical normal distributions of the damage site size are shown. Following additional loading cycles there will be an increase in microdamage, either through an increase in the number of microdamage sites (blue, dashed line) or an increase in the size of microdamage sites (red, dotted line).

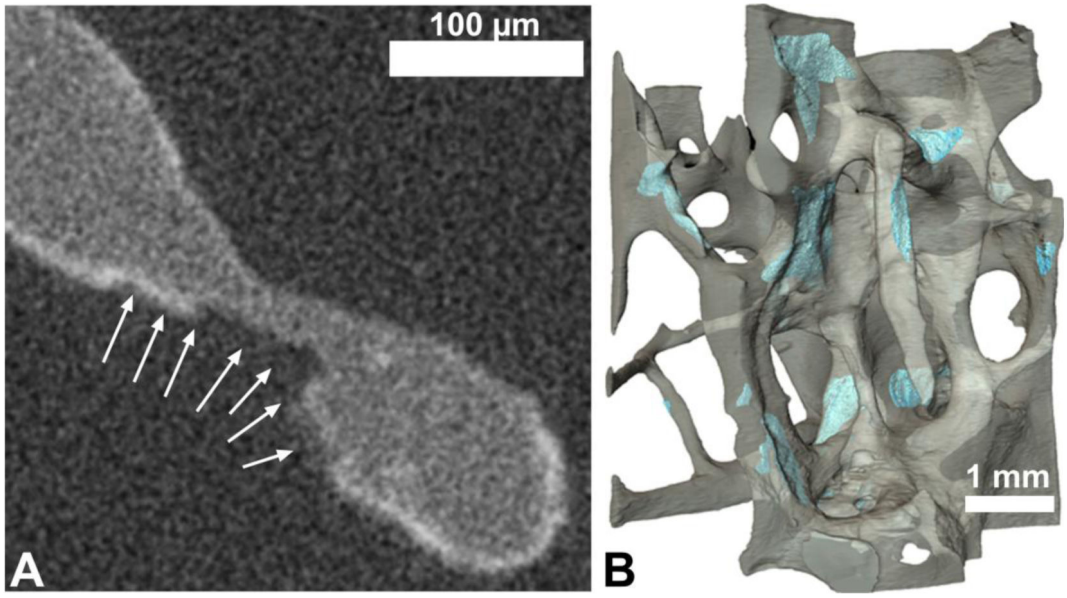

Figure 3.

(A) Resorption cavities were initially identified in two-dimensional micro-computed tomography images by finding eroded surfaces (arrows) and then (B) traced on three dimensional reconstructions of the micro-computed tomography images (blue).

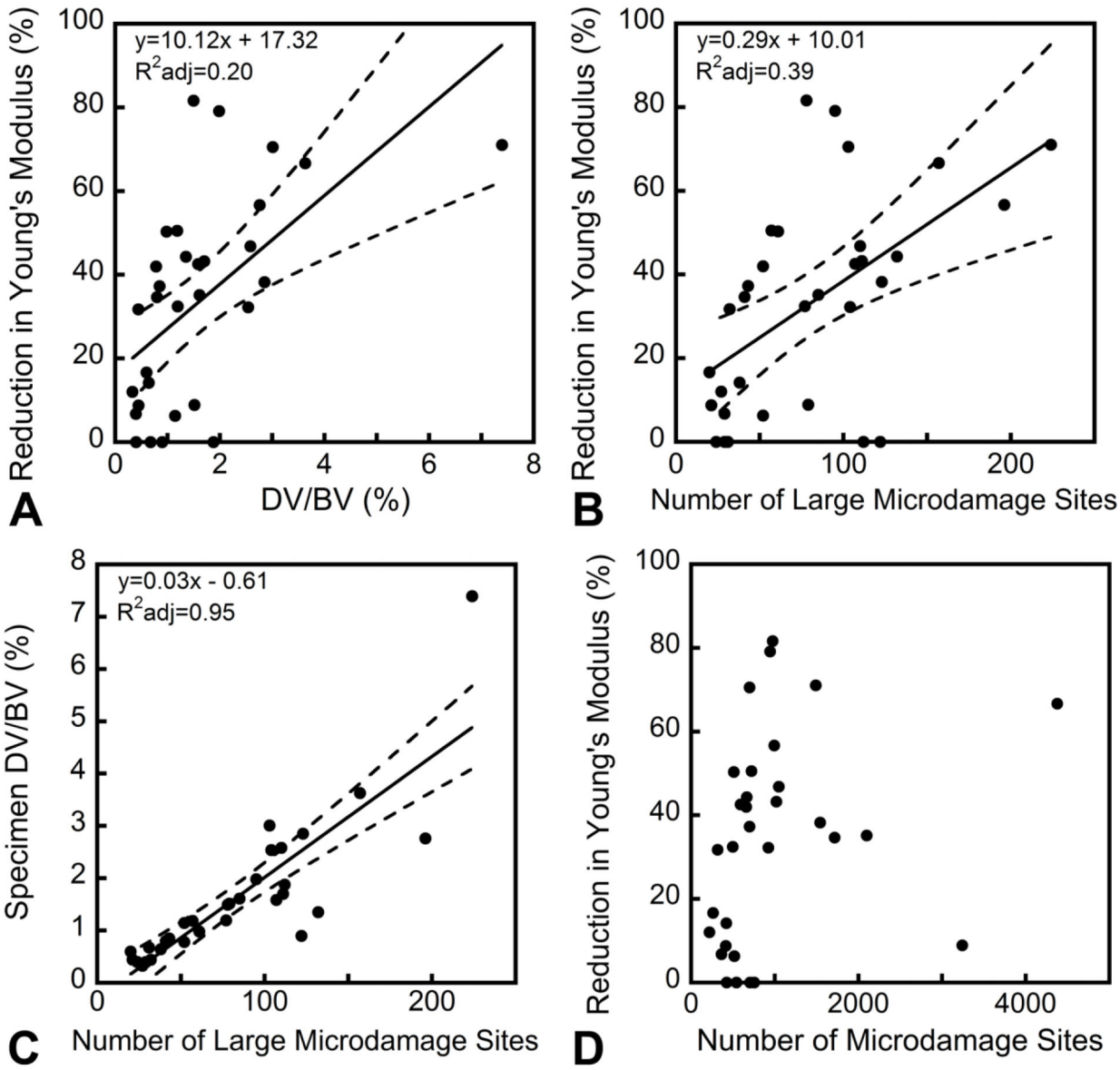

Figure 4.

Although the overall damage volume fraction (DV/BV) was correlated with the reduction in Young's modulus (A), the number of large microdamage sites showed a stronger correlation to the reduction in Young's modulus (B). The number of large microdamage sites was also correlated with the overall damage volume fraction (C). The overall number of microdamage sites was not correlated with the reduction in Young's modulus (D).

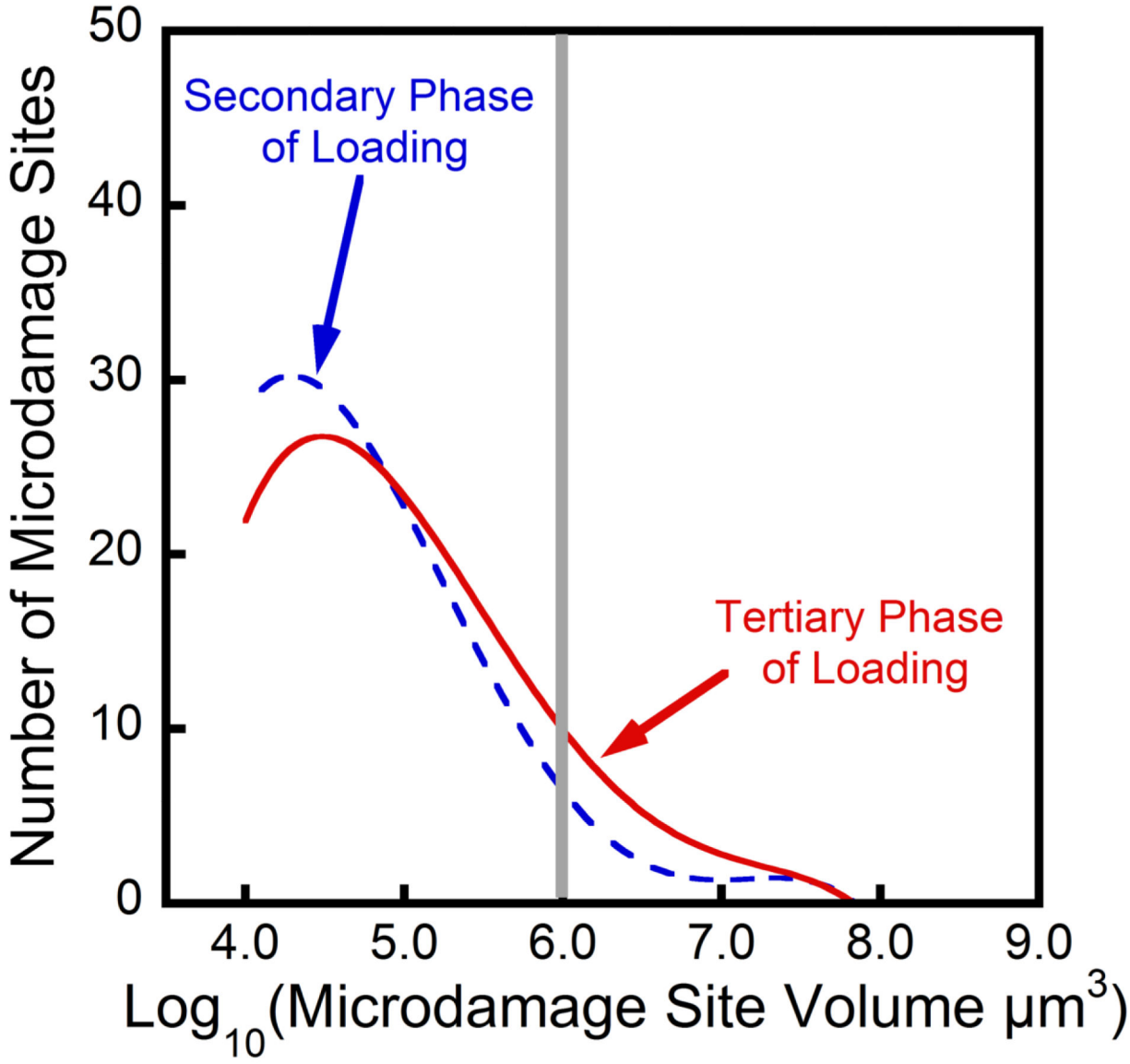

Figure 5.

Representative histograms of the microdamage site volumes in a specimen loaded to the secondary phase of fatigue life (dashed blue) and that of a specimen loaded to the tertiary phase of fatigue life (solid red) are shown. The grey line shows the cutoff we used for defining large microdamage sites (sites larger than 10^6 μm^3). The specimen loaded to the tertiary phase displayed more microdamage sites classified as large than the specimen loaded to the secondary phase.

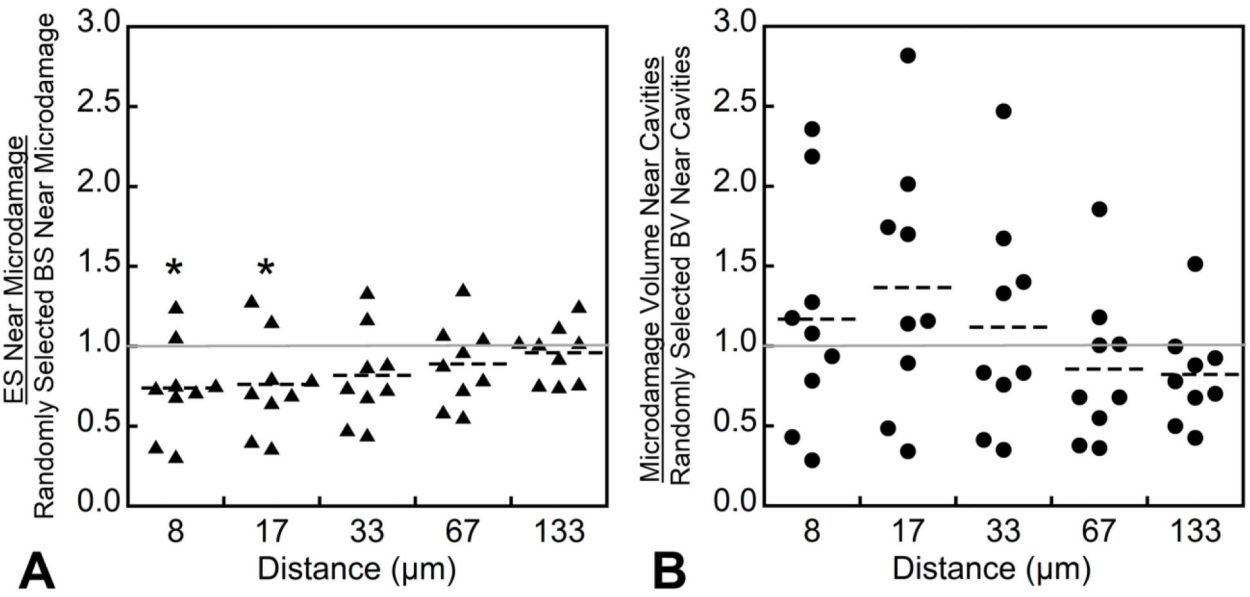

Figure 6.

The spatial correlations between microdamage sites and resorption cavities using the volume based method are shown. A value of 1.0 indicates no spatial correlation and a value less than 1.0 indicates a negative correlation. (A) An eroded surface was less likely to be near microdamage than regions of bone surface selected at random (at a distance of 8 and 17 μm). (B) No significant spatial correlations were observed when using microdamage as the predictor.

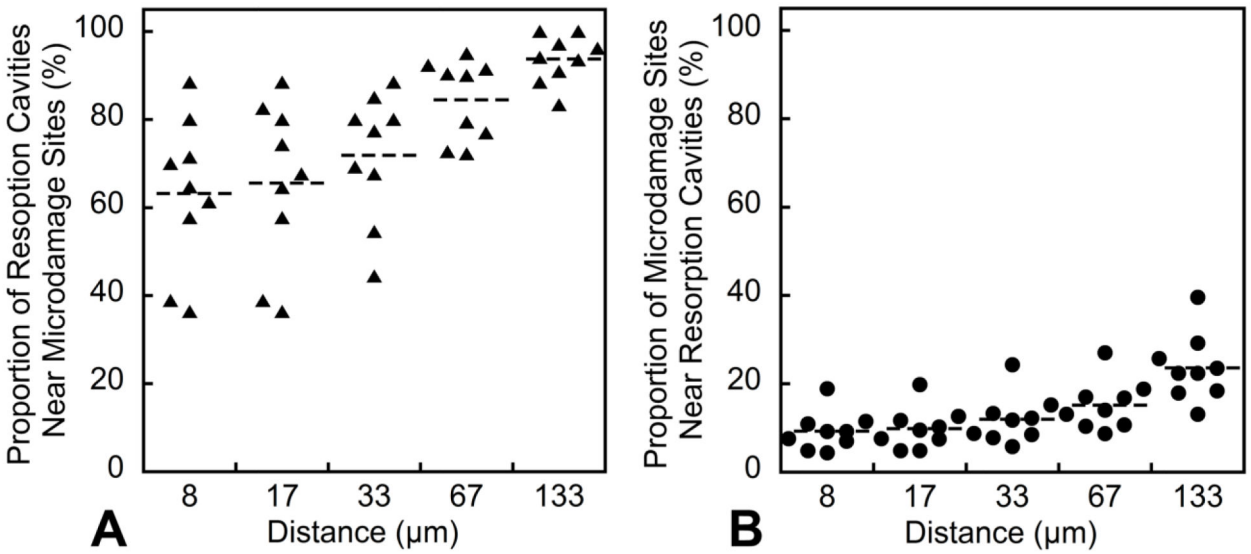

Figure 7.

The spatial correlations between microdamage sites and resorption cavities using the object based method are shown. While the majority of resorption cavities were near microdamage sites (A), few microdamage sites were near resorption cavities (B).